Faraday Discussions
Cite this: DOI: 10.1039/d4fd00160e

PAPER

View Article Online
View Journal

Terrestrial and marine sources of ice nucleating particles in the Eurasian Arctic†

Guangyu Li, ‡*[a] André Welti, [b] Arianna Rocchi,[c] Germán Pérez Fogwill,[b] Manuel Dall'Osto[c] and Zamin A. Kanji *[a]

Received 1st October 2024, Accepted 29th November 2024
DOI: 10.1039/d4fd00160e

Ice nucleating particles (INPs) catalyze primary ice formation in Arctic low-level mixed-phase clouds, influencing their persistence and radiative properties. Knowledge of the abundance and sources of INP over the remote Arctic Ocean is scarce due to limited data coverage, particularly in the Eurasian Arctic. This study presents summertime measurements of INP concentrations in seawater, fog water and air from the ship-based Arctic Century Expedition, exploring the Barents, Kara, and Laptev Seas, and the adjacent high Arctic islands and archipelagos in August and September 2021. Heat sensitivity tests of ambient aerosols revealed that heat-liable, biogenic INPs make up the majority of Arctic INP populations at temperatures above −20 °C, and to a lesser extent down to −25 °C. INP content in fog water is found to be similar to ambient aerosol, indicating that INP in marine air could also act as cloud condensation nuclei. Measurements of aerosolized INPs using an on-board sea-spray aerosol bubble tank generator exhibit a positive correlation with ambient INP concentrations, but not with INP abundance in seawater samples. INP concentrations in air derived from sea water samples (using a NaCl conversion factor representative for the Arctic) were significantly lower than those measured in ambient air or bubble tank experiments. INP concentrations in bubble tank experiments positively correlated with the phosphate and fluorescence signals in the water. This suggests an important role of the aerosolization mechanism for preferentially partitioning biogenic INPs to the atmosphere.

1 Introduction

Ice nucleating particles (INPs) trigger primary ice formation in mixed-phase clouds (MPCs), which modulate the cloud radiative and microphysical

[a]Institute for Atmospheric and Climate Science, ETH Zurich, Switzerland. E-mail: lgy526462219@gmail.com; zamin.kanji@env.ethz.ch
[b]Finnish Meteorological Institute, Helsinki, Finland
[c]Department of Marine Biology and Oceanography, Institute of Marine Sciences (ICM, CSIC), Barcelona, Spain
† Electronic supplementary information (ESI) available. See DOI: https://doi.org/10.1039/d4fd00160e
‡ Now at: Laboratory for Microwave Spatial Intelligence and Cloud Platform, Deqing Academy of Satellite Applications, Deqing, China.

properties.[1,2] Accurate simulations of cloud properties in climate models require a realistic representation of INPs.[3] The concentration of INPs influences the number, size, and phase partitioning of hydrometeors in clouds, which in turn affect the cloud albedo, lifetime, and might impact precipitation patterns. In the Arctic, cloud cover impacts the regional energy balance while the amount of snow-producing clouds affects the formation of sea ice. A scarcity of INP observations limits our understanding of the abundance and sources of INPs in different environments. The Eurasian Arctic Ocean is of particular interest because it could be the source of highly active INPs.[4]

INPs can originate from terrestrial and marine sources. Mineral dust particles are a significant terrestrial source, capable of initiating ice nucleation (IN) at temperatures lower than approximately −15 °C.[5] Known sources of mineral dust near the Arctic Ocean include the Arctic coasts of Greenland,[6] the Russia coast,[4] glacial outwash plains in Svalbard,[7] and sandy deserts on Iceland.[8] Marine INP sources in the Arctic Ocean are related to sea-spray aerosol (SSA), generated through wave breaking and bubble bursting, which represents another crucial source of INPs in the high-latitude Arctic Ocean.[9–12] The production rate of SSA varies with meteorological conditions (*e.g.*, wind speed, and sea surface temperature[13,14]) and sea ice coverage.[13] Also both the abundance of different components in seawater and the aerosolization process at the ocean–atmosphere interface impact aerosol emission and partitioning.[12,15] In addition to inorganic sea salt and sulfate, SSA contains marine biogenic aerosol, which can be composed of particulate microbes, phytoplankton cell exudates,[16,17] and dissolved organic macromolecules[18] released during phytoplankton blooms. These components can be IN-active at temperatures as high as −5 °C.[19] It is hypothesized that the emission of IN-active marine biogenic aerosol could coincide with marine phytoplankton blooms and co-emission of biogenic aerosol precursors, such as dimethyl sulfide (DMS) and chlorophyll-*a*.[20–22] As the Arctic warms and sea ice retreats, marine biological processes are likely to become more active which could change the marine INP emission. Uncovering the sources and understanding the mechanisms of marine biogenic aerosol release into the atmosphere is therefore needed for predicting the abundance of Arctic low-level MPCs in the future.[23,24]

In this work, we present ship-borne measurements of INP concentrations (N_{INP}) sampled from different environments (seawater, fog water, marine air, and air from a bubble tank generator) and related aerosol properties during the Arctic Century Expedition in the summer of 2021 over the Barents, Kara and Laptev Seas and the adjacent high Arctic islands and archipelagos in the Eurasian Arctic, a region that has not been studied before.

2 Methods

2.1 Campaign overview

The Arctic Century Expedition took place from 5th August to 6th September 2021, starting and ending at the port of Murmansk, Russia. Fig. 1 shows the location of experiments, instruments and samplers on board the research vessel (RV) *Akademik Tryoshnikov* reported in this work. Detailed information on instrument configurations and their functions in each sector is given in Table 1. For measurements on the 1st deck, an aerosol generation bubble tank (BT) system for

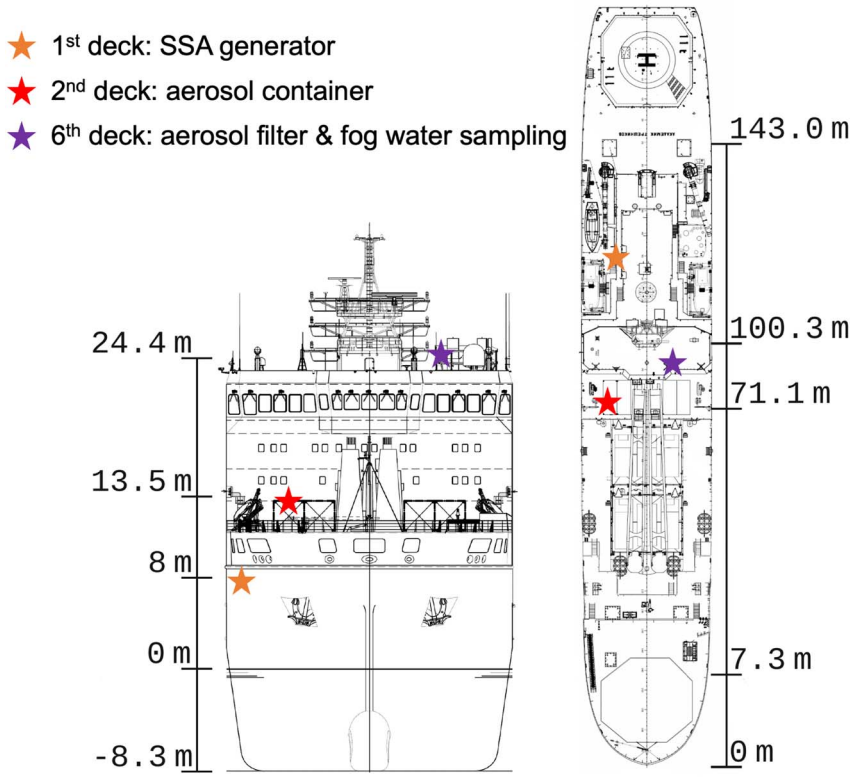

Fig. 1 Position of instrumentation on board of the *RV Akademik Tryoshnikov* (adapted from vessel plans by the Arctic and Antarctic Research Institute). Height is provided relative to the approximate water line in the front view (left panel), and distance from the ship's bow in the top view (right panel). A SSA bubble tank generator was operated on the 1st deck, online measurement equipment for aerosol characterization was located on the 2nd deck, and aerosol sample collector and fog water sampler were installed on the 6th deck.

controlled SSA generation was set up. Inside the BT, aerosol is generated by simulating the bubble-bursting mechanisms using water jets to create bubbles. Water samples include 32 L seawater collected at 2 m depth with Niskin bottles using a Conductivity–Temperature–Depth (CTD) rosette sampling system or freshwater samples collected on land using sampling buckets (see sampled water locations in Fig. 2). The SSA generated in the BT was collected on filters for N_{INP} measurements, and characterized for the size distribution by a scanning mobility particle sizer (SMPS) and an optical particle counter (OPC). Fresh and seawater samples used for BT experiments were also filtered for biochemical analysis (see Rocchi *et al.*[25] for details on BT experiments and analysis of biological variables). On the 2nd deck, an aerosol container configured as a laboratory included interval sampling of ambient aerosol by a liquid impinger (for INP analysis), and continuous characterization of particle size distributions with an SMPS and an aerodynamic particle sizer (APS). On the 6th deck, several fog water collectors were installed next to a low volume PM_{10} filter sampler (LVS) (Table 1). The LVS sampled ambient aerosol continuously for 12 h per filter along the ship track

Table 1 Overview of instrumentation set-up on the *RV Akademik Tryoshnikov* during the Arctic Century Expedition (for the onboard location, see Fig. 1)

On-board location	Instrument	Temporal resolution	Flow rate	Function
1st deck	CTD-rosette	Station-based	—	Seawater sampling
	Aerosol generator (BT)	Station-based	—	Aerosol generation from sampled water
	SMPS (BT-aerosol)	4 min	0.6 L min^{-1}	Online particle size distribution (<0.6 μm)
	OPC (BT-aerosol)	5 s	2.83 L min^{-1}	Online particle size distribution (>0.3 μm)
	Water filter	Station-based	—	Water filtration for biochemical analysis
	BT aerosol filter	6–20 h	10 L min^{-1}	Aerosol collection on filters for offline INP analysis
2nd deck	Impinger	3 h	300 L min^{-1}	Aerosol collection in water for offline INP analysis
	SMPS	4 min	0.6 L min^{-1}	Ambient particle size distribution (0.012–0.6 μm)
	APS	4 min	1 L min^{-1}	Ambient particle size distribution (0.5–20 μm)
6th deck	Fog water collector	6–12 h	—	Fog water collection for offline INP analysis
	LVS (PM_{10} inlet)	12 h	38.3 L min^{-1}	Aerosol collection on filters for offline INP analysis

during the campaign. The fog water and filters were analyzed for INPs in the laboratory after the campaign. Additionally, several near-shore surface microlayer (SML) and underlying subsurface seawater (SSW) samples were collected. The locations of fog water, sea- and freshwater, SML and SSW samples are marked in Fig. 2. Detailed experimental setups for sample collections and measurements are described in the following section.

2.2 Sample collection

2.2.1 Ambient aerosol samples. From the aerosol container laboratory on the 2nd deck, ambient aerosols were collected (3 times a day for 3 hours) each into 15 mL ultra-pure water (W4502-1L, Sigma-Aldrich) using a high flow-rate impinger (Coriolis® μ, Bertin Instruments, with a lower limit aerodynamic cut-off size of 0.5 μm) at a flow rate of 300 L min^{-1}. On the 6th deck, aerosol particles were collected onto 47 mm polycarbonate membrane filters (Whatman, 0.4 μm pore size) using the LVS (Model DPA14, Digitel) with a PM_{10} inlet. In the following, these filter samples are referred to as LVS filters. The LVS inlet was approximately 25 m above sea level. The operating flow rate was maintained at 38.3 L min^{-1} for 12 hours sampling intervals. The sampling was temporarily

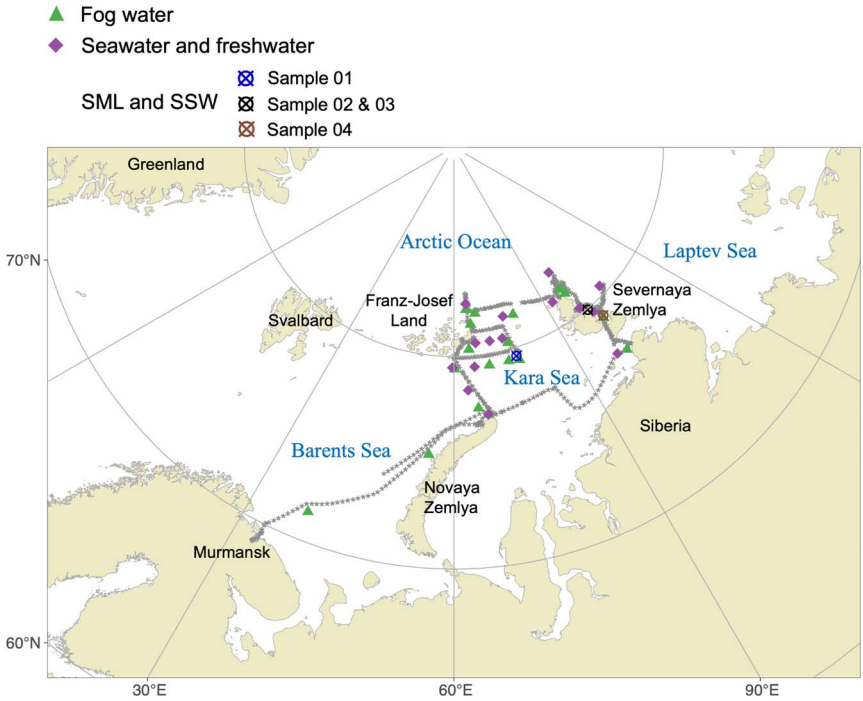

Fig. 2 Map of water sampling locations during the Arctic Century Expedition. The gray asterisks represent the ship's track (1 h interval) throughout the expedition.

halted when the wind direction was detected to originate from the ship's chimney, in order to prevent contamination from exhaust emissions. The impinger and LVS filter samples were stored at −20 °C on board and for transport until they were used for the INP analysis after the campaign back at the laboratory at ETH Zurich. During the campaign, a total of 75 impinger and 50 LVS filter samples were collected.

2.2.2 Aerosol samples collected from BT. The BT aerosol generation system[26] was used to characterize aerosols produced from bubble bursting. The BT consists of a 60 L stainless-steel cylindrical tank. For operation, the BT was filled with 30 L of water collected either with the CTD-rosette (sea water) or on islands (island run-off or freshwater). Water in the BT was circulated to the top *via* a peristaltic pump and showered back to the water surface as plunging jets at a flow rate of 12 L min^{-1}. The spray aerosol forms at the water surface *via* bubble bursting.[15] Particle-free air was supplied into the tank headspace at 60 L min^{-1} to prevent aerosol from concentrating (see Rocchi *et al.*[25] for detailed experimental setup). Two frequently regenerated diffusion dryers were used to dry the water spray aerosol for particle size distribution measurements and filter collection. 47 mm polycarbonate membrane filters (Whatman, 0.4 μm pore size) were used to collect aerosols generated from the BT. The sample flow rate was approximately 10 L min^{-1} for a duration of 6 to 20 hours. BT filters were stored frozen at −20 °C until INP analysis was conducted back in the laboratory at ETH Zurich. The INP concentration measured from ambient aerosols and aerosolization from BT were not corrected for freezing point depression, following the representation of

atmospheric immersion freezing occurring in dilute cloud droplets with water activity ~ 1.

2.2.3 Environmental water samples. A total of 21 fog water samples were collected using the instruments shown in Fig. 3a. An array of 7 cactus-like collectors were fixed by the white clamps and mounted on the railing at the 6th deck on board. Once covered in fog, the fog water/frost deposits onto the sharp tips of the "cactus" and drips down/melts into a glass bottle attached at the bottom.

To compare any enrichment of INPs between the sea surface microlayer (SML, a sub-millimeter layer located at the interface between the ocean and atmosphere) and subsurface water (SSW), seawater was sampled at the coastal regions (see Fig. 2) accessed by a helicopter. Four SML samples were collected following the procedure shown in Fig. 3b. A clean glass plate is repeatedly vertically submerged and withdrawn from the sea surface to collect SML samples.[27] The thin microlayer film attached to the plate is then transferred into sample bottles using a Teflon scraper to wipe down the glass plate. Four SSW bulk seawater samples were sampled by directly submerging sample bottles to about 50 cm below the ocean surface in parallel to the SML sampling.

For BT experiments, 30 L (of the sampled 32 L) of either sea or freshwater was used for aerosol generation. The 13 seawater samples were collected from a depth

Fig. 3 (a) Fog water sample collector; (b) collection of SML.

of 2∼4 m using the uppermost Niskin bottle from a SEA-BIRD CTD rosette sampling system. The 3 freshwater samples were collected using a plastic bucket from an island river, island lake, and island runoff (at the shore of Pioneer Island, October Revolution Island, and a lake on Cape Baranov, respectively, see Fig. 2). 2 L of each water sample was filtered to analyze biogeochemical variables.[25] All samples (fog water, SML and SSW, water filters, water filtrates, and unfiltered water) were stored frozen at −20 °C until analyses.

Conductivity was measured prior to analyzing the INP concentrations for seawater samples to account for the freezing point depression from dissolved sea salt. The corrected freezing temperature was calculated according to Koop and Zobrist,[28] and following the procedure of Wilson *et al.*[10]

2.3 INP analysis with DRoplet Ice Nuclei Counter Zurich (DRINCZ)

Aqueous particle suspensions were used for immersion-mode INP analysis using DRINCZ.[29] After frozen storage, impinger samples were allowed to melt at 4 °C overnight before analysis. Membrane filter samples were immersed in 10 to 15 mL ultra-pure water and agitated using a sonicator for 30 min to resuspend the particles from filters into the water. Each liquid sample was pipetted into a Polymerase Chain Reaction (PCR) tray with 96 aliquots of 50 μL and cooled in an ethanol bath at 1 °C min^{-1}. Freezing events were detected optically from the change in transparency of an aliquot upon freezing. INP concentration (N_{INP}) was derived from the frozen fraction of aliquots at each integer temperature following Vali.[30] For aerosol samples collected by impinger and LVS filters, N_{INP} is calculated as per volume of sampled air:

$$N_{INP,air}(T) = -\frac{\ln\left[1 - \frac{N_{frz}(T)}{N_{tot}}\right]}{V_{aliquot}} \cdot \frac{V_{water}}{V_{flow}} \quad (1)$$

where $N_{INP}(T)$ is the INP concentration at temperature T, $N_{frz}(T)$ is the number of frozen aliquots at temperature T, N_{tot} is the total number of aliquots ($N_{tot} = 96$), $V_{aliquot}$ is the aliquot volume ($V_{aliquot} = 50$ μL). V_{water} is the total water volume of the impinger sample or the volume of water used to suspend LVS filters, and V_{flow} is the sampled air volume, which is the product of the sampling flow rate and sampling time. For the fog, fresh and seawater samples, N_{INP} is quantified as per volume of sampled water:

$$N_{INP,water}(T) = -\frac{\ln\left[1 - \frac{N_{frz}(T)}{N_{tot}}\right]}{V_{aliquot}} \quad (2)$$

The N_{INP} in fog water was converted to N_{INP} in air:

$$N_{INP,air}(T) = N_{INP,fog\ water}(T) \cdot F_{fog,air} \quad (3)$$

where $F_{fog,air}$ is the liquid water content (LWC) of fog water in g m^{-3} converted to a volume of water in the air. For simplification, $F_{fog,air}$ was taken from fog layer measurements of Costabloz *et al.*[31] who reported a LWC of 0.1 g m_{air}^{-3} for fog up to 50 m above ground.[31] The conversion factor from per volume of liquid to per volume of air is $F_{fog,air} = 1 \times 10^{-7}$ $L_{fog\ water}$ L_{air}^{-1}.

Field blanks undergoing the same procedures as the samples were collected every three days during the campaign. The N_{INP} were corrected for the background of the blanks according to Vali,[32] by subtracting the differential INP spectrum of the blanks from the samples. Based on the limit of detection (LOD) from the collected sample volume and the purity of the nano-pure water, the highest temperature for N_{INP} detection was approximately −5 °C (above which sampled air volumes are deemed too low to detect any INPs), and the lowest temperature at which N_{INP} can be reliably reported is −25 °C (below which nano-pure water initiates freezing). The overall uncertainty of the reported freezing temperatures is ±0.9 °C.[29]

2.4 Heat treatment of INP samples

Macromolecules originating from biological species (*e.g.*, bacteria and phytoplankton) typically comprised of proteins can effectively catalyze ice nucleation[33] and are heat labile. Heating effectively unfolds the proteinaceous structure, degrading their IN ability.[33,34] In the post-campaign heat treatment, liquid samples extracted from the 50 LVS filters were subjected to 95 °C for 20 min. After cooling to room temperature, the samples were redistributed to PCR trays for INP analysis using DRINCZ. By comparing the IN activity before and after heating, it is possible to assess the contribution of heat-labile species to the INP population, which is a proxy to indicate the presence of biological INPs.[33]

2.5 Particle size distribution

In the aerosol container laboratory on the 2nd deck, the size distribution of submicron ambient aerosol was measured using an SMPS (Model 3938, consisting of a 3082 classifier, a 3081 long differential mobility analyzer, and a 3787 Condensation Particle Counter, TSI Inc.). The SMPS operated at a sampling flow rate of 0.6 L min^{-1} with a sheath-to-sample ratio of 10 : 1, covering a size range of approximately 12 to 600 nm in electrical mobility diameter. A charge correction was applied to account for the misclassification of larger particles carrying multiple charges. Concurrently, the size distribution of coarse-mode particles (ranging from approximately 0.5 to 20 μm in aerodynamic diameter) was monitored using an APS (Model 3321, TSI Inc.) at a flow rate of 1 L min^{-1}. Both the SMPS and APS were synchronized to a time resolution of 4 minutes to ensure aligned size distributions. The electrical mobility diameters obtained from the SMPS and aerodynamic diameters from the APS were converted to volume-equivalent diameters, assuming an average particle density of 2 g cm^{-3}.[7,35]

To monitor the aerosol size properties generated from the BT experiments, particle size distribution measurements were conducted using a combination of an SMPS and an OPC (Model GT-526S, MetOne). Two diffusion dryers filled with silica gel were used to dry the particles before entering the SMPS and the OPC. The SMPS was configured the same as in the aerosol container. The OPC provided 6-binned particle count in optical diameter (*i.e.*, >0.3 μm, >0.5 μm, >1 μm, >2.5 μm, >5 μm and >10 μm) to extend the range of size distributions.

2.6 Chemical composition analysis

Inductively coupled plasma-optical emission spectrometry (ICP-OES, Model 5100, Agilent Technologies) was used to detect 11 selected elements (Al, Ca, Cl, Fe, K,

Mg, Mn, Na, P, S, Si) in the 75 aerosol suspension samples collected by the impinger. The impinger samples were diluted by a factor of 10 with 2% HNO_3 solution prior to the chemical analysis. Quality control was established by the measurement of blank samples and standard reference materials of each element processed in parallel (see details of experimental protocols in Gilli *et al.*[36]). The resulting elemental concentrations for Cl, Fe, Mn, and K were below the LOD and thus are not discussed. The remaining elements were analyzed in this work, including P, S, and joint classes of AlSiCa and NaMg, representing dust and sea salt components, respectively, according to the standards introduced in Hiranuma *et al*.[37]

A total of 16 water samples (13 seawater + 3 freshwater) used for BT experiments were collected (including water filters, water filtrates and unfiltered water) for subsequent quantification of a series of biogeochemical variables, including chlorophyll-*a* (Chl-*a*), fluorescence, glucose, dissolved organic carbon (DOC), total dissolved nitrogen (TDN) and inorganic components, *e.g.*, nitrate (NO_3^-), phosphate (PO_4^{3-}) and silicate. For Chl-*a* measurements, the sample was extracted from filters using 90% acetone for photometric analyses. Fluorescence was measured with a fluorescence probe installed on the downward cast of the CTD-rosette. Samples for DOC and TDN were collected in combusted glass ampoules (8 h, 500 °C) and subsequently acidified with 85% phosphoric acid, heat sealed immediately, and stored at 4 °C in the dark until analysis by applying the high-temperature catalytic oxidation method.[38] More detailed analytical procedures are described in Rocchi *et al.*[25] and von Jackowski *et al*.[39]

2.6.1 Back trajectory analysis and sea ice conditions. Back trajectories of air parcels were computed to identify the origin of the air masses. Two-day (48 h) backward trajectories were calculated with the Lagrangian analysis tool LAGRANTO[40,41] using the three-dimensional wind fields from the hourly ERA5 reanalysis (5th generation of ECMWF atmospheric reanalysis of the global climate covering the period from January 1950 to the present, Hersbach *et al.*[42]) interpolated on a regular horizontal grid of 0.5° horizontal spacing. The trajectories started at hourly intervals along the ship track and were selected at sea level (approximately 1000 hPa). To analyze the origin of the INPs, air parcels showing surface precipitation below the air parcel position >0.1 mm h^{-1} were removed along each trajectory. During these situations INPs are expected to be removed and, thus, source contributions are neglectable. Additionally, ERA5 hourly data with a 30 km grid on sea ice coverage was used to characterize the sea ice conditions.

3 Results and discussion

3.1 INPs in different Arctic environments

3.1.1 INPs in the ambient air. The contribution of heat-labile and stable INPs to the N_{INP} at different temperatures in the ambient air during the Arctic Century 2021 campaign was tested by heating the washing water of LVS filter samples. Fig. 4a presents the cumulative INP spectra of each LVS filter sample before and after heating it to 95 °C for 20 min. The overall N_{INP} was reduced by approximately one order of magnitude for all samples at all temperatures after heating. The degradation of N_{INP} is most pronounced at temperatures higher than −15 °C. Fig. 4b shows that the reduction in N_{INP} above −15 °C is close to 100%, indicating

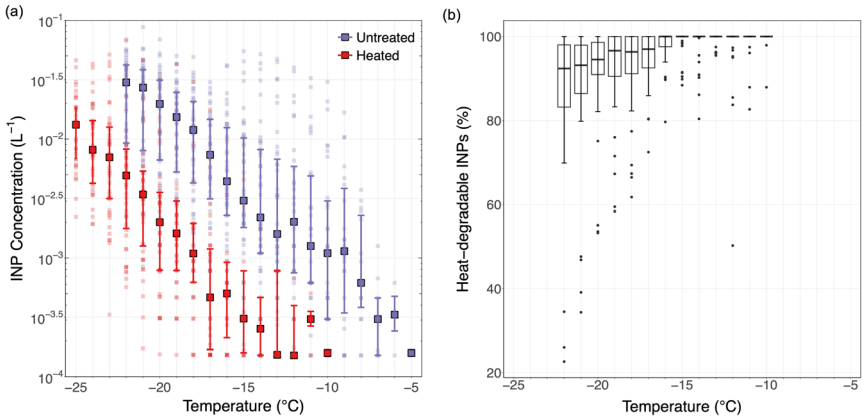

Fig. 4 (a) Ambient INP concentration measured from LVS filters as a function of temperature with and without heat treatment. The light-shaded data points show individual measurements, and the dark data points in blue and red are median N_{INP} before and after heat treatment, respectively. The lower and upper bound of whiskers are the 25% and 75% quantiles of the observations. (b) Boxplot showing the contribution of heat-degradable INPs. The lower and upper bounds of the boxes indicate the 25% and 75% quantiles of N_{INP}, and the horizontal line within the boxes represents the median value. The whiskers have a length of 1.5 × IQR (interquartile range), and individual points are outliers.

a high abundance of heat-labile, IN-active proteins or biological macromolecules in all samples.[33,43] These results support previous findings[16,44–46] that biological INPs are a significant source of INPs over the Arctic Ocean. Several samples exhibit a lower reduction in N_{INP} at $T < -20$ °C, suggesting an increasing fraction of heat-resistant INPs towards lower temperatures, such as larger aggregates of ice-nucleating macromolecules or mineral dust.[47]

3.1.2 INPs in fog water. Fog can act as an intermediate reservoir in the atmospheric lifecycle of INPs, potentially influencing the distribution and availability of INPs for cloud formation.[23] Fig. 5 shows the cumulative spectra of N_{INP} measured from a total of 21 fog water samples collected in the current study. Overall, the N_{INP} measured from fog water is in the middle range of the concentration measured for ambient INPs. This is in contrast to previous findings that showed enrichment of INPs in fog water[8,23,49] attributed to INP scavenging by fog droplets. The larger surface size of fog water droplets relative to ambient aerosols can enhance the scavenging of INPs from the ambient air through collision and coagulation. Additionally, the relatively slow dissipation of fog provides an extended residence time of INPs within the fog droplets,[49] leading to a concentrated population of INPs in the fog water compared to the ambient air. It is surprising that we don't observe this enrichment for more samples. This can be explained by the calm conditions present during fog, where the flux of INPs from the ocean to the boundary layer is low, or could indicate that our assumption of the fog water content is too low. However, derived N_{INP} from the "fog20" sample matches the concurrently sampled ambient INP concentration (shown in pink triangles) quite well. This is also true for the lowest INP measured in the "fog15" sample when compared to the ambient INP from the LVS samples (shown in brown triangles). The overlap of N_{INP} in fog water and LVS filter samples indicates

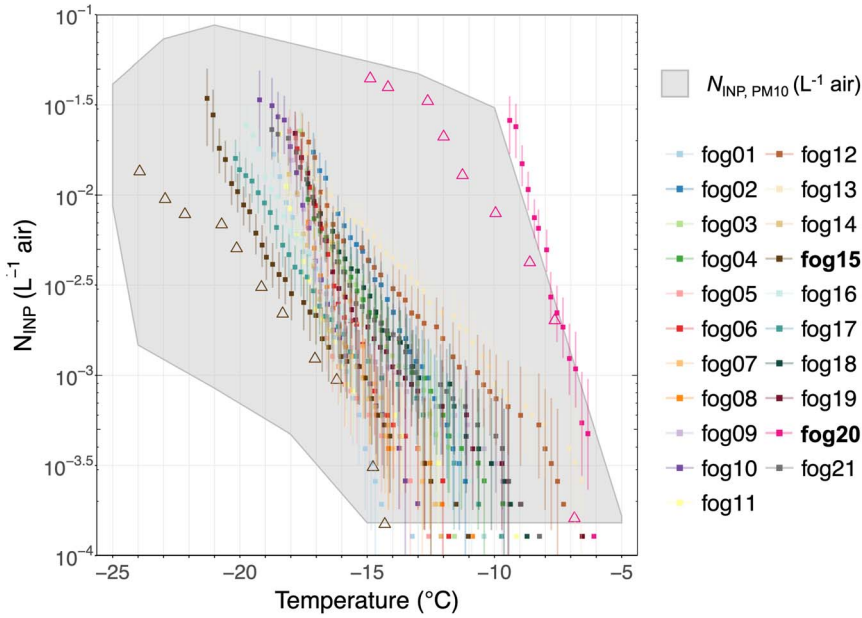

Fig. 5 Cumulative INP spectra of fog water samples compared with ambient INP concentration measured from LVS filters. N_{INP} in fog water was derived by converting to N_{INP} in air using a fog water content of 0.1 g m_{air}^{-3} (Costabloz *et al.*,[31] see Section 2.3 for details). The error bars show the 95% confidence intervals derived following Agresti and Coull.[48] The triangles represent the N_{INP} measured by the LVS concurrently with "fog15" and "fog20".

that a particular enrichment of INPs in fog water compared to fog-free air was not observed. The match in INP concentrations shown between ambient and fog water for "fog15" and "fog20" indicates that INPs are also cloud condensation nuclei. The observed N_{INP} from filters therefore represent N_{INP} that could be active in MPCs where INP first have to act as cloud condensation nuclei before triggering immersion freezing.

N_{INP} in the fog water varies by a factor of 5 to 10 at $T < -15$ °C. The variation becomes larger at warmer temperatures, primarily due to the higher uncertainty from the low number of active INPs at higher temperatures. However, this variation is constrained compared to N_{INP} in ambient aerosol. One reason for the lower variability in N_{INP} could be that ambient air is often influenced by long-range transport of INPs from diverse sources, which results in a larger natural variability in N_{INP} depending on the atmospheric conditions in the boundary layer and air mass history. Also enhanced random dilution could broaden the N_{INP}. The ambient N_{INP} was positively correlated (moderate to strong) with N_{INP} in concurrent fog water samples (results shown in Table A1 in the ESI†), which suggests that their sources overlap but some differences still exist. In particular, the highest correlation was observed for N_{INP} at −20 °C. At these temperatures, mineral dust (from long-range transport) is IN-active or heat resistant silicates from biogenic sources could contribute to both INPs in fog water and ambient INPs. The lower correlation at higher temperatures suggests different dominant INP sources at these temperatures for ambient and fog water samples.

The sample "fog20" (Fig. 5) exhibited the highest N_{INP} compared to the other samples. To better understand the characteristics of this sample, we plot the 2 days air mass backward trajectories for the high ("fog20") and low ("fog15") N_{INP} samples in Fig. 6 together with the sample collection period and location. For "fog20", the ship traveled in the middle of Severnaya Zemlya and the North Siberia Peninsula during the sampling period where local terrestrial sources of INPs are in the vicinity of the ship-track (see pink "fog20" trajectory in Fig. 6). The air mass history indicates that the North Siberia Peninsula could provide terrestrial INP active at high temperatures (below −6 °C) *via* long-range transport even when the ship moved away from land. Considering the season of the measurements (August/September), thawing permafrost could be one source of INPs.[50,51] In addition, mineral dust from the coast of the North Siberia Peninsula and fluvial sediment input into the ocean from the many Siberian rivers could be resuspended from the ocean surface[52] and contribute to the high N_{INP} in sample "fog20". In contrast, for the low-N_{INP} sample "fog15", the ship was located north of Franz-Josef Land, spending some time within the pack-ice. The air masses originated from the central Arctic a region completely covered by sea ice, which besides INP released from sublimating blowing snow, lacks significant sources of INPs.

Admittedly, the 48 hours time frame with 0.5° spatial resolution is appropriate for tracking air mass movements from nearby sources but may not capture the

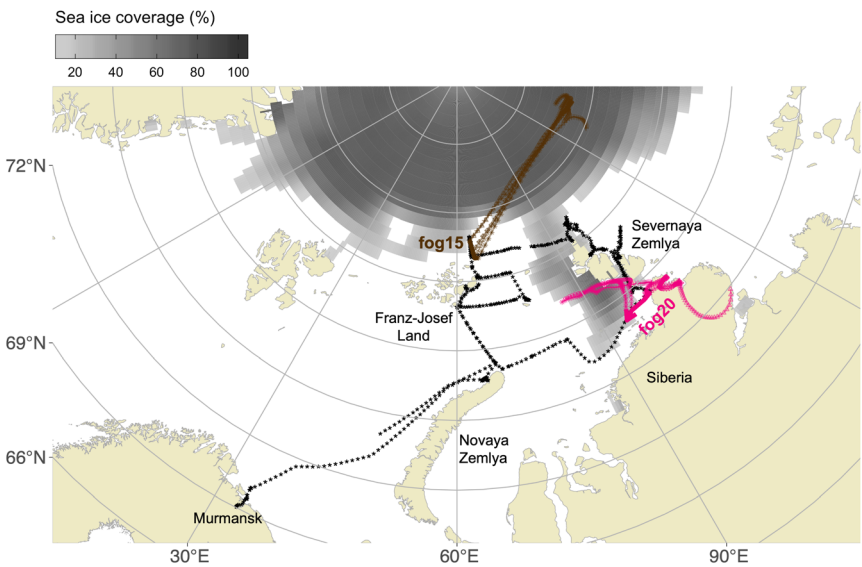

Fig. 6 2 Day backward trajectories from the ship location at sea level. The black asterisks represent the ship's track throughout the entire expedition. The percentage of sea ice coverage is shown in gray scale. Back trajectories covering the fog sampling period, starting from the ship's location at sea level, are launched every 3 hours, with the points along the trajectory indicating hourly intervals. The solid thick lines and arrows indicate the ship's movement during the overlapping period where "fog15" and "fog20" were collected from 06:00 to 18:00 on 17th August 2021 close to the ice edge north of Franz-Josef Land, and 18:00 on 31st August 2021 to 06:00 UTC on 1st September 2021 in between Severnaya Zemlya and Siberia, respectively.

influence of long-range transport or finer-scale variability. As a limitation, longer trajectories (*e.g.*, 72–96 hours) could provide insights into potential distant sources but may introduce uncertainties in Arctic regions due to rapid changes in meteorological conditions. Additionally, while the trajectory analysis offers insights into general air mass origins, it does not allow for precise attribution of specific INP sources, especially in complex regions where terrestrial and marine influences converge.

3.1.3 INPs in seawater. To understand the relative abundance of INPs in different layers of seawater, N_{INP} in SML and SSW samples were measured. For samples 2 and 3 collected east of Severnaya Zemlya in the Laptev Sea, no difference was found in N_{INP} between the SML and SSW samples. For sample 04 (SML_04 *vs.* SSW_04 in Fig. 7) the N_{INP} was slightly higher in the SML than SSW. Overall, samples 02, 03, and 04, which were collected in the same region showed

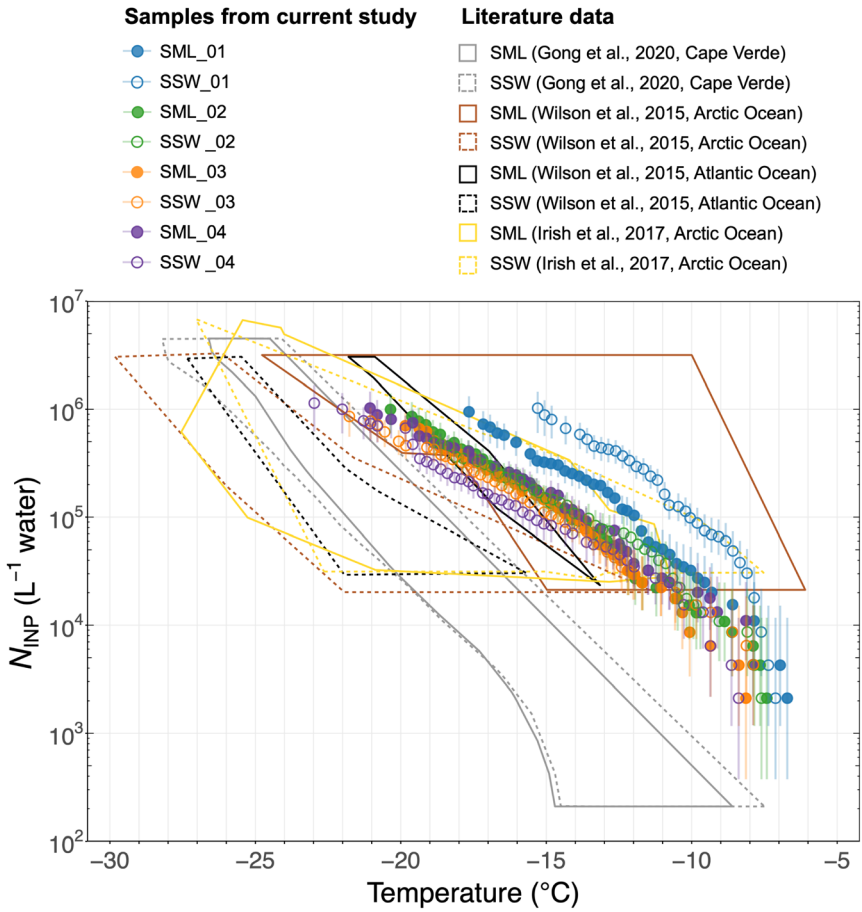

Fig. 7 Cumulative INP spectra of sea surface microlayer (SML) and subsurface seawater (SSW) samples. Error bars show the 95% confidence intervals. Literature data[10,53,54] of previous measurements of N_{INP} in seawater at different locations are shown for comparison. The freezing temperatures for seawater N_{INP} are corrected for freezing point depression.

very similar N_{INP}. Previous studies, *e.g.* ref. 10, observed that the SML is enriched in organic material from biological components of the ocean and is more IN-active than SSW. Observations in the European Arctic and North Atlantic Ocean showed that N_{INP} correlated with organic material in SML. However, the sampling conditions of the SML and SSW can influence the results. In our samples, N_{INP} was higher in the SSW than SML for sample 01 collected east of Wiese Island in the Kara Sea. During the collection of SML_01 and SSW_01, it was observed that water was very turbid due to outflow of sediment from the nearby Wiese Island. More sediment was present in sample SSW_01 than SML_01, explaining the higher N_{INP} in SSW_01 than SML_01. In the previous studies of Gong *et al.*,[53] both an enrichment and a decline of INPs in the SML compared to SSW were observed in Cape Verde. On the other hand, Irish *et al.*[54] did not find enrichment in the SML compared to SSW from Arctic Ocean samples. There is no universal INP enrichment in the SML, despite it being rich in organic components. The different results from past studies and the varied results in our 4 samples can be attributed to the limited number of samples for a given sampling condition. Specifically, the frequency of marine biological activity (*e.g.*, a phytoplankton bloom) in different ocean layers,[10,55] uncertain mixing of the sea surface,[54–57] ocean state (*e.g.*, wind speed[44,55] and sea surface temperature[58,59]), all affect the SML partitioning process leading to a variable enrichment factor of INPs in the sampled SML. Production of SSA is typically associated with strong wind speeds, white cap formation, and wave breaking.[14,60] As such these conditions represent turbulent conditions where the SML and SSW are significantly more mixed than in calmer conditions. To quantify the INP flux from the ocean, aerosolization of the ocean surface water is necessary (see Section 3.2), but assuming the sources are only from the surface-rich microlayer may lead to biases, especially for SSA production in coastal areas where sediments are re-suspended with the SSA.[52]

3.2 Ocean–atmosphere partitioning of INPs

From the isolated experiments of different water samples in the BT, we distinguish the abundance of INPs generated by spray aerosolization of the water samples based on the sampling location. Fig. 8 shows the INP spectra of aerosolized particles from the BT experiments ($N_{INP,BT}$). Overall, freshwater samples that were collected from rivers and lakes on islands (labeled as "Island water bodies") and seawater samples collected close-to-islands produced higher aerosolized N_{INP} compared to seawater samples farther away from land (see Fig. 8) supporting strong terrestrial INP sources. The "island water bodies" showing the lowest freezing temperature (Land_075BIS) was sampled on Pioneer Island in the bay in brackish waters as revealed by the intermediate salinity level (see Table A3 in the ESI†). The Land_080 sample was a seawater sample directly in contact with land. Given the highest INP concentrations were observed for samples with zero and high salinity (Land_078 and Land_080, respectively), the contact to land appears to control the INP concentrations observed rather than the salinity level. The influence of salinity is further discussed in later sections. From the seawater samples collected at different locations, $N_{INP,BT}$ was highest for samples obtained close to islands. For seawater samples, reduced $N_{INP,BT}$ was associated with increased sea ice coverage, *i.e.*, $N_{INP,BT}$ produced from samples collected in the open ocean contained more INPs than samples from within the MIZ/ice pack.

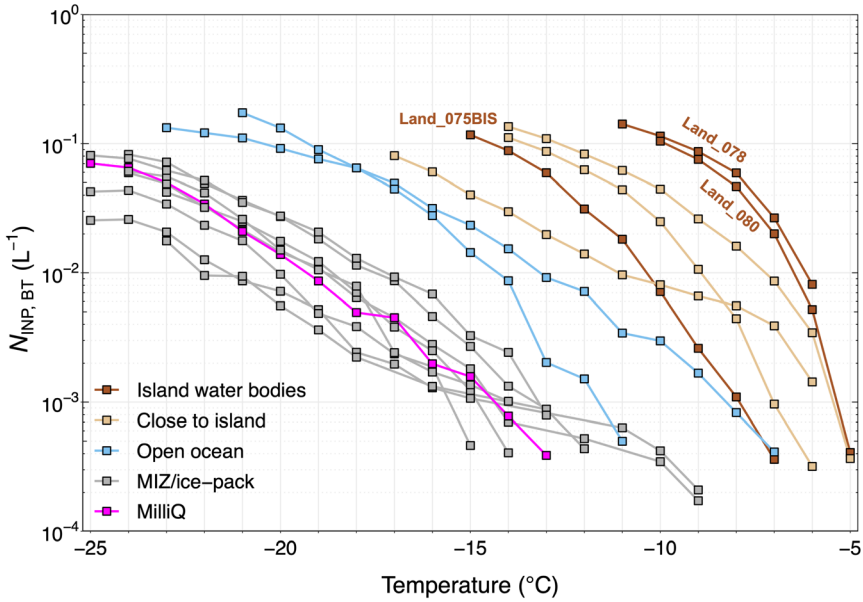

Fig. 8 Cumulative INP spectra for BT-generated particles, classified according to the sampling location. "Island water bodies" indicates water collected from island rivers and lakes, "MilliQ" denotes a reference experiment with pure water. All other categories are seawater samples. "Close to island" indicated that the ship location was less than 15 km from the coastline.

In Fig. 9 the $N_{INP,BT}$, ambient N_{INP} (from LVS filters) and N_{INP} in air derived from the SML and SSW samples are shown. To convert the N_{INP} in the SML and SSW samples to that in air, a factor of 10^{-10} was used that represents the ratio of NaCl in the atmosphere to that in seawater for the Arctic.[61] First, we note that the BT-generated INPs overlap strongly with the ambient measurements. This suggests that the ambient INP has strong local sources from the seawater. Due to increased mixing and dilution in the ambient, it is also expected that $N_{INP,BT}$ would be biased higher in the BT than in the ambient as seen in Fig. 9. Secondly, the N_{INP} derived for SML and SSW are much lower than those measured in ambient air and in the BT. This strongly supports the fact that the aerosol production mechanisms that occur at the sea surface (and in the BT) are responsible for preferentially partitioning INPs to the airborne phase. Modeling the bubble or jet bursting process at the sea surface is crucial to capture the true flux of INPs from the ocean to the atmosphere since the enrichment of airborne INPs cannot simply be represented by the mass transfer of NaCl.

3.3 Correlations of N_{INP} with SSA size and bio-chemical seawater properties

Fig. 10 shows the correlation between a selection of variables measured from the BT experiments during the Arctic Century campaign. Spearman rank correlation coefficients were calculated due to the unknown distribution of each investigated parameter. Notably, $N_{INP,BT}$ negatively correlates with salinity, reflecting INP-rich island water bodies. In addition, weak to moderate correlations were found between $N_{INP,BT}$ and seawater temperature ($T_{seawater}$). This could be a purely

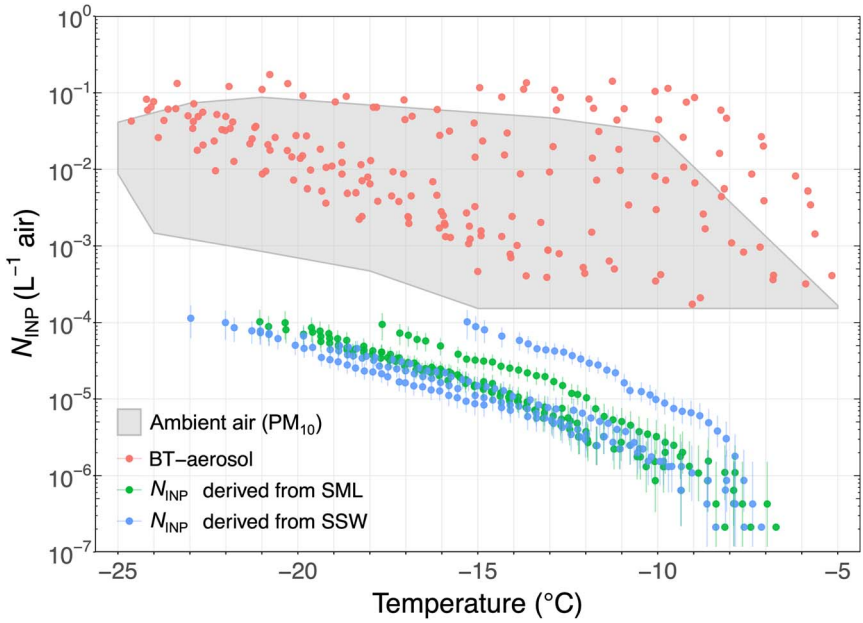

Fig. 9 Atmospheric N_{INP} as a function of temperature measured from ambient air by LVS filter with the PM_{10} inlet (gray shaded area), BT-aerosol collected on filters (red), and N_{INP} derived from SML (green) and SSW (blue) samples, respectively. The factor used to convert N_{INP} in the SML and SSW samples to concentration in air is 10^{-10}.[53]

latitudinal or seasonal effect. However, higher water temperature is reported to boost marine biological productivity by lowering the activation energy of enzymes,[62] thereby increasing the emission of IN-active marine biogenic aerosol.

Concentrations of several components were measured for the water samples used in the BT experiments. Fig. 10 shows some overall positive and significant correlations were found between $N_{INP,BT}$ and chl-*a* (except $T = -15$ °C), fluorescence and phosphate. Although neither of these components is reported to be IN-active, their abundance is a tracer of promoted marine biological activity, from which IN-active organics and biogenic exudates can originate. Recently it was shown that fluorescent particle concentrations are a good predictor for INPs of dust and biological origin.[63] No clear correlation between $N_{INP,BT}$ and DOC was found in contrast to McCluskey *et al.*[18] who suggested that a positive correlation is indicative of sub-0.2 μm DOC components acting as marine INPs. Strong correlations were also not observed between $N_{INP,BT}$ and TDN and NO_3^-. A significant and moderate correlation was found between $N_{INP,BT}$ and silicate concentration. A biological origin of silicate in the ocean from marine diatoms and microalgae with siliceous cells has been reported (*e.g.*, *Thalassiosira pseudonana*) to be IN-active.[17] Another possibility for the positive correlation with silicate is the presence of dust-type INPs. Cornwell *et al.*[52] showed in a laboratory study that the seawater doped with dust can be re-aerosolized with retained IN activity and added to the atmospheric INP populations during bubble bursting. This pathway of INP transfer could be responsible for the relatively high N_{INP} aerosolized from

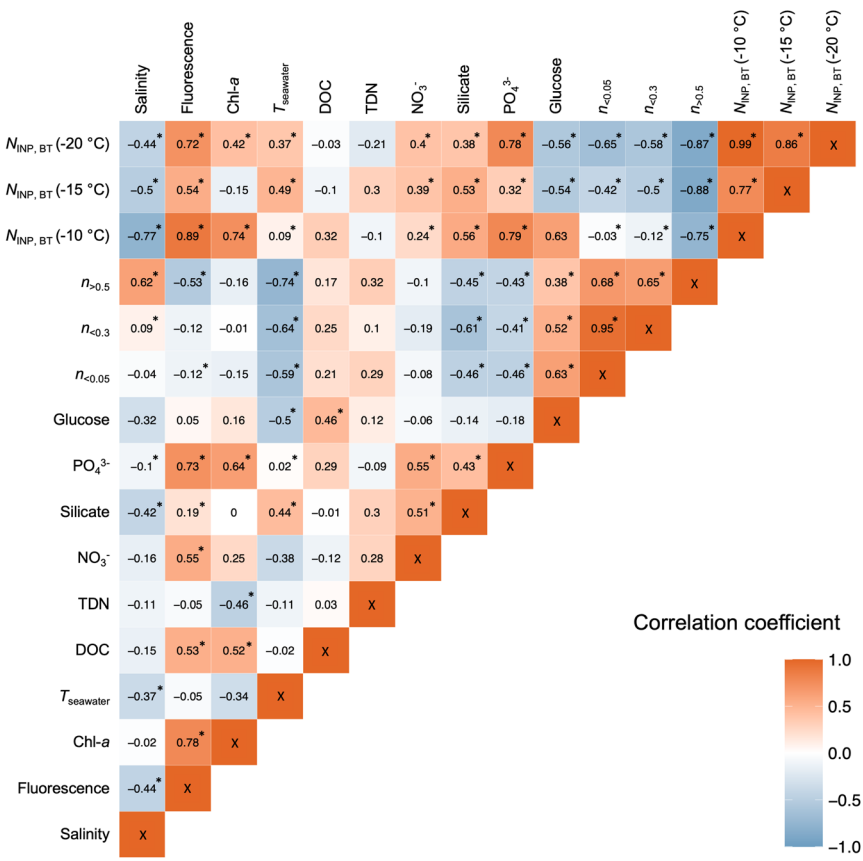

Fig. 10 Spearman rank correlation matrix of variables measured from the BT experiments during the Arctic Century campaign, with the coefficients shown in each box. The cross-correlated parameters are $N_{INP,BT}$ measured at three selected temperatures ($T = -10$, -15 and -20 °C); the salinity and temperature of water samples ($T_{seawater}$) used for BT experiments; and quantity of nutrients and biological and terrestrial source indicators measured from the water samples, including chlorophyll-*a* concentration, fluorescence, concentrations of glucose, dissolved organic carbon (DOC), total dissolved nitrogen (TDN), nitrate (NO_3^-), phosphate (PO_4^{3-}) and silicate. Additionally, the number concentration of aerosolized particles with diameters >0.5 μm measured from the OPC ($n > 0.5$), $n < 0.3$ and $n < 0.05$ measured from SMPS were cross-compared. The asterisks represent results with statistical significance ($p < 0.05$). Smoothed time stamps (in minutes) were applied to different data sets for correlation analyses.

land-sourced freshwater or seawater samples collected approaching islands (see Fig. 8) that are often rich in suspended sediments due to the fluvial outwash.

$N_{INP,BT}$ is negatively correlated with particle concentrations $n > 0.5$ aerosolized from the water samples, indicating that the absolute loading of SSA (dominated by NaCl) does not determine the abundance of aerosolized INPs (supporting the conclusions from Fig. 9) and emphasizes that N_{INP} cannot always be predicted by aerosol number concentration[35] like parameterizations for dusty or highly polluted atmospheres.[64–66] However, the negative correlation between $N_{INP,BT}$ and

$n < 0.3$ and $n < 0.05$ do not support that finer aerosol mode could be used as predictors for INP concentrations. The absence of a positive correlation with aerosol number concentration of different size ranges strengthens our conclusion that N_{INP} cannot always be predicted by aerosol number concentrations in agreement with studies elsewhere in the Arctic and other remote regions.[35,67,68] Combining the correlation analyses of $N_{INP,BT}$ with biological indicators (*i.e.*, Chl-*a*, fluorescence, PO_4^{3-}) and silicate, we infer that the aerosolization processes at the water–air interface preferentially partitions the IN-active species to the aerosol phase and that the composition (phosphate, silicate) and fluorescence information are crucial to predict INP concentrations.[63]

The relative abundance of INPs in different samples taken simultaneously including ambient air (impinger samples), seawater samples (CTD seawater), and BT-aerosolized SSA are shown in Fig. 11. The comparison reveals insignificant correlations between N_{INP} in ambient air and the coincidentally sampled seawater (Fig. 11a). In contrast, a statistically significant correlation was found between airborne ($N_{INP,ambient}$) and BT-aerosolized ($N_{INP,BT}$) INP concentrations at the selected freezing temperatures (Fig. 11b). $N_{INP,BT}$ are present in higher concentrations compared to ambient INPs by about an order of magnitude due to the absence of dilution in the BT-aerosolized air. The positive correlations suggest that the BT experiments simulate a realistic aerosolization process at the sea–air interface, and the seawater can be a considerable source of INPs in the Arctic Ocean. The data from Fig. 11b suggest that SSA is a source of INPs, but the absence of a positive correlation with N_{INP} derived from seawater in Fig. 11a suggests otherwise. This additional support is that the missing factor for water samples is the aerosolization process that enriches INPs in the air, which cannot simply be accounted for by the flux of SSA from water to air. The mechanisms of INP aerosolization at the ocean–air interface could be impacted by several compounding factors, *e.g.*, an enrichment of INPs at the sea surface microlayer,[10]

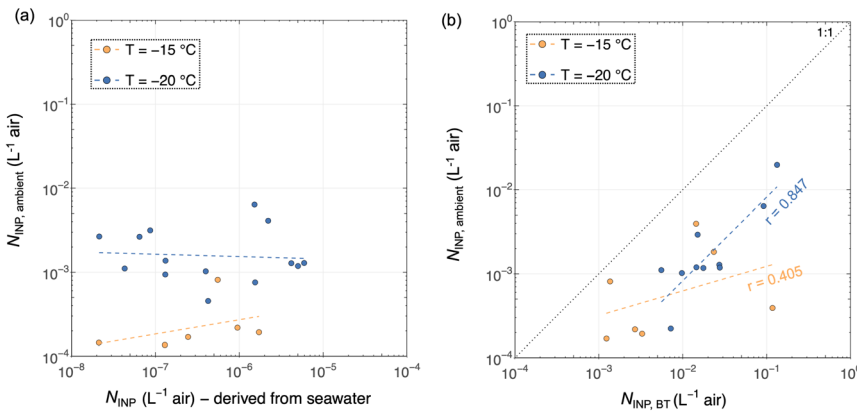

Fig. 11 Comparisons between ambient N_{INP} measured from impinger samples and coincident N_{INP} measured from (a) seawater and (b) BT-aerosol filters. The dashed lines indicate the linear regression in the logarithmic scale, and only the statistically significant ($p < 0.05$) r values (correlation coefficients) are shown in the figure. The correlation coefficients of all data are given in Table A1.†

dissolved species and their abundance,[27,69] biological productivity,[16,21] sea surface temperature,[27,59] wind speed,[70] and sea ice concentrations.[20]

4 Conclusions

This study presents summertime observations of N_{INP} and aerosol related properties over the Barents, Kara, and Laptev Seas in the Eurasian Arctic from August to September 2021. Variability in N_{INP} is highly influenced by local sources, and to some extent meteorological conditions, and potentially long-range transport. A series of online and offline measurements were applied to investigate the INP abundance in seawater, fog, and ambient air to understand the sources of the INP and production mechanisms.

The majority of ambient aerosol samples collected on LVS filters were prone to degradation in INP concentration after heating to 95 °C for 20 min, indicating the presence of proteinaceous or biogenic INPs that are heat-labile. By comparing N_{INP} in the ambient air to other environments, similar N_{INP} was observed in fog water compared to ambient air, indicating INPs are not enriched in fog water and are likely cloud condensing nuclei. INPs in fog should be considered in studies of INP distribution and availability due to its role as an intermediate reservoir and for the formation of ice fogs in the atmospheric lifecycle of INPs. No clear trend was observed for INP enrichment in the SML compared to SSW, which is both in agreement with and in contrast to previous studies. The frequency of marine biological activity, such as phytoplankton blooms, fluvial input of sediment INPs, along with the variability in sea surface mixing and ocean state, could influence the abundance of INPs in different ocean layers.

A comparison of N_{INP} in the SML, SSW and CTD seawater samples to *in situ* aerosol measurements from a BT system and ambient INPs from the LVS filters reveals that the bubble-bursting mechanism is important in transferring INPs from the ocean to the atmosphere. The abundance of INPs in the BT-sprayed aerosols showed a dependence on the composition of water components, with terrestrial freshwater possessing higher N_{INP} compared to seawater samples. In accordance, a reduced $N_{INP,BT}$ was associated with a longer distance to land or an increased sea ice coverage where the subsurface seawater samples were collected. Based on the correlation analyses between $N_{INP,BT}$ and biological activity, this study supports the important role of marine biogenic aerosol as a source of INPs in the remote Arctic Ocean far from terrestrial sources. Our results highlight key relationships, such as the strong correlation between INP abundance and local biogenic factors (*e.g.*, chlorophyll and fluorescence signals). These correlations suggest that integrating real-time biological activity data, especially during phytoplankton blooms, could improve model parameterizations of Arctic INP emissions. Lastly, other effects may be present in addition to the composition during the SSA generation and INP partitioning in the ocean and atmosphere, including the enrichment of IN-active materials in the sea surface microlayer, sea ice coverage, advection, and mixing in different ocean layers.

Data availability

The data in this article are available at **https://doi.org/10.3929/ethz-b-000717415**.

Author contributions

GL performed sample processing and data analysis, produced figures, interpreted results, and co-wrote the manuscript. GL and AW participated in the campaign and conducted *in situ* sampling and measurements. AW contributed to the manuscript preparation and acquired funding. AR conducted the aerosol generation bubble tank experiment and collected samples for biochemical analysis. GPF performed INP analysis and heat treatment of filter samples, CTD seawater samples, and BT-aerosolized filter samples. MD provided the research idea on INP partitioning using the INP results from the bubble tank. ZAK supervised the project, obtained funding, and was involved in experiment and campaign planning, data interpretation, and manuscript writing. All authors reviewed the manuscript.

Conflicts of interest

The authors declare that no competing interests are present.

Acknowledgements

This research used samples and/or data provided by the Arctic Century Expedition, a joint initiative led by the Swiss Polar Institute (SPI), the Antarctic and Arctic Research Institute (AARI), and GEOMAR Helmholtz Centre for Ocean Research Kiel (GEOMAR), and funded by the Swiss Polar Foundation. GL and ZAK acknowledge that this project has been made possible by a grant from the Swiss Polar Institute, Dr Frederik Paulsen. GPF acknowledges funding from the Academy of Finland (Grant No. 342227). ZAK acknowledges this project has received funding from the Horizon Europe program under Grant Agreement No. 101137680 (Project CERTAINTY). We acknowledge all those involved in the fieldwork associated with the Arctic Century Expedition, including technical support from Dr Michael Rösch. We acknowledge Dr von Jackowski and Dr Engel for sharing biogeochemical data of CTD water samples. We acknowledge Franziska Aemisegger and Iris Thurnherr calculated the backward trajectories used in this study. We would like to thank Dr Xu from ETH for providing the ICP-OES instrument with assistance on sample preparation and measurements.

References

1 A. Korolev, G. McFarquhar, P. R. Field, C. Franklin, P. Lawson, Z. Wang, E. Williams, S. J. Abel, D. Axisa, S. Borrmann, J. Crosier, J. Fugal, M. Krämer, U. Lohmann, O. Schlenczek, M. Schnaiter and M. Wendisch, Mixed-phase clouds: Progress and challenges, *Meteorol. Monogr.*, 2017, **58**, 1–50, DOI: **10.1175/AMSMONOGRAPHS-D-17-0001.1**.

2 M. C. Serreze and R. G. Barry, Processes and impacts of Arctic amplification: A research synthesis, *Glob. Planet. Change*, 2011, 77(1–2), 85–96, DOI: **10.1016/j.gloplacha.2011.03.004**.

3 B. J. Murray, K. S. Carslaw and P. R. Field, Opinion: Cloud-phase climate feedback and the importance of ice-nucleating particles, *Atmos. Chem. Phys.*, 2021, **21**(2), 665–679, DOI: **10.5194/acp-21-665-2021**.

4 G. C. E. Porter, M. P. Adams, I. M. Brooks, L. Ickes, L. Karlsson, C. Leck, M. E. Salter, J. Schmale, K. Siegel, S. N. F. Sikora, M. D. Tarn, J. Vüllers, H. Wernli, Z. Paul, J. Zinke and B. J. Murray, Highly active ice-nucleating particles at the summer North Pole, *J. Geophys. Res.:Atmos.*, 2022, **127**(6), e2021JD036059, DOI: **10.1029/2021JD036059**.

5 C. Hoose and O. Möhler, Heterogeneous ice nucleation on atmospheric aerosols: a review of results from laboratory experiments, *Atmos. Chem. Phys.*, 2012, **12**(20), 9817–9854, DOI: **10.5194/acp-12-9817-2012**.

6 G. Li, E. K. Wilbourn, Z. Cheng, J. Wieder, A. Fagerson, J. Henneberger, G. Motos, R. Traversi, S. D. Brooks, M. Mazzola, S. China, A. Nenes, U. Lohmann, N. Hiranuma and Z. A. Kanji, Physicochemical characterization and source apportionment of Arctic ice-nucleating particles observed in Ny-Ålesund in autumn 2019, *Atmos. Chem. Phys.*, 2023, **23**, 10489–10516, DOI: **10.5194/acp-23-10489-2023**.

7 Y. Tobo, K. Adachi, P. J. DeMott, T. C. J. Hill, D. S. Hamilton, N. M. Mahowald, N. Nagatsuka, S. Ohata, J. Uetake, Y. Kondo and M. Koike, Glacially sourced dust as a potentially significant source of ice nucleating particles, *Nat. Geosci.*, 2019, **12**, 253–258, DOI: **10.1038/s41561-019-0314-x**.

8 A. Sanchez-Marroquin, O. Arnalds, K. J. Baustian-Dorsi, J. Browse, P. Dagsson-Waldhauserova, A. D. Harrison, E. C. Maters, K. J. Pringle, J. Vergara-Temprado, I. T. Burke, J. B. McQuaid, K. S. Carslaw and B. J. Murray, Iceland is an episodic source of atmospheric ice-nucleating particles relevant for mixed-phase clouds, *Sci. Adv.*, 2020, **6**(26), eaba8137, DOI: **10.1126/sciadv.aba8137**.

9 C. Leck and E. K. Bigg, Biogenic particles in the surface microlayer and overlaying atmosphere in the central Arctic Ocean during summer, *Tellus B*, 2005, **57**(4), 305–316, DOI: **10.3402/tellusb.v57i4.16546**.

10 T. W. Wilson, L. A. Ladino, P. A. Alpert, M. N. Breckels, I. M. Brooks, J. Browse, S. M. Burrows, K. S. Carslaw, J. A. Huffman, C. Judd, W. P. Kilthau, R. H. Mason, G. McFiggans, L. A. Miller, J. J. Nájera, E. Polishchuk, S. Rae, C. L. Schiller, M. Si, J. V. Temprado, T. F. Whale, J. P. S. Wong, O. Wurl, J. D. Yakobi-Hancock, J. P. D. Abbatt, J. Y. Aller, A. K. Bertram, D. A. Knopf and B. J. Murray, A marine biogenic source of atmospheric ice-nucleating particles, *Nature*, 2015, **525**(7568), 234, DOI: **10.1038/nature14986**.

11 J. M. Creamean, R. M. Kirpes, K. A. Pratt, N. J. Spada, M. Maahn, G. de Boer, R. C. Schnell and S. China, Marine and terrestrial influences on ice nucleating particles during continuous springtime measurements in an Arctic oilfield location, *Atmos. Chem. Phys.*, 2018, **18**(24), 18023–18042, DOI: **10.5194/acp-18-18023-2018**.

12 K. A. Prather, C. D. Hatch and V. H. Grassian, Analysis of atmospheric aerosols, *Annu. Rev. Anal. Chem.*, 2008, **1**(1), 485–514, DOI: **10.1146/annurev.anchem.1.031207.113030**.

13 P. K. Quinn, D. B. Collins, V. H. Grassian, K. A. Prather and T. S. Bates, Chemistry and related properties of freshly emitted sea spray aerosol, *Chem. Rev.*, 2015, **115**(10), 4383–4399, DOI: **10.1021/cr500713g**.

14 H. Grythe, J. Ström, R. Krejci, P. Quinn and A. Stohl, A review of sea-spray aerosol source functions using a large global set of sea salt aerosol concentration measurements, *Atmos. Chem. Phys.*, 2014, **14**(3), 1277–1297, DOI: **10.5194/acp-14-1277-2014**.

15 C. O'Dowd, D. Ceburnis, J. Ovadnevaite, J. Bialek, D. B. Stengel, M. Zacharias, U. Nitschke, S. Connan, M. Rinaldi, S. Fuzzi, *et al.*, Connecting marine productivity to sea-spray *via* nanoscale biological processes: Phytoplankton dance or death disco?, *Sci. Rep.*, 2015, **5**(1), 14883, DOI: **10.1038/srep14883**.

16 J. M. Creamean, J. N. Cross, R. Pickart, L. McRaven, P. Lin, A. Pacini, R. Hanlon, D. G. Schmale, J. Ceniceros, T. Aydell, N. Colombi, E. Bolger and P. J. DeMott, Ice nucleating particles carried from below a phytoplankton bloom to the Arctic atmosphere, *Geophys. Res. Lett.*, 2019, **46**(14), 8572–8581, DOI: **10.1029/2019GL083039**.

17 D. A. Knopf, P. A. Alpert, B. Wang and J. Y. Aller, Stimulation of ice nucleation by marine diatoms, *Nat. Geosci.*, 2011, **4**(2), 88–90, DOI: **10.1038/ngeo1037**.

18 C. S. McCluskey, J. Ovadnevaite, M. Rinaldi, J. Atkinson, F. Belosi, D. Ceburnis, S. Marullo, T. C. J. Hill, U. Lohmann, Z. A. Kanji, C. O'Dowd, S. M. Kreidenweis and P. J. DeMott, Marine and terrestrial organic ice-nucleating particles in pristine marine to continentally influenced northeast Atlantic air masses, *J. Geophys. Res.:Atmos.*, 2018, **123**, 6196–6212, DOI: **10.1029/2017JD028033**.

19 B. J. Murray, D. O'Sullivan, J. D. Atkinson and M. E. Webb, Ice nucleation by particles immersed in supercooled cloud droplets, *Chem. Soc. Rev.*, 2012, **41**(19), 6519–6554, DOI: **10.1039/C2CS35200A**.

20 A. Gabric, P. Matrai, G. Jones and J. Middleton, The nexus between sea ice and polar emissions of marine biogenic aerosols, *Bull. Am. Meteorol. Soc.*, 2018, **99**(1), 61–81, DOI: **10.1175/BAMS-D-16-0254.1**.

21 M. Rinaldi, S. Fuzzi, S. Decesari, S. Marullo, R. Santoleri, A. Provenzale, J. von Hardenberg, D. Ceburnis, A. Vaishya, C. D. O'Dowd and M. C. Facchini, Is chlorophyll-*a* the best surrogate for organic matter enrichment in submicron primary marine aerosol?, *J. Geophys. Res.:Atmos.*, 2013, **118**(10), 4964–4973, DOI: **10.1002/jgrd.50417**.

22 S. Becagli, C. Ghedini, S. Peeters, A. Rottiers, R. Traversi, R. Udisti, M. Chiari, A. Jalba, S. Despiau, U. Dayan and A. Temara, MBAS (methylene blue active substances) and LAS (linear alkylbenzene sulphonates) in Mediterranean coastal aerosols: Sources and transport processes, *Atmos. Environ.*, 2011, **45**(37), 6788–6801, DOI: **10.1016/j.atmosenv.2011.04.041**.

23 L. Ickes, G. C. E. Porter, R. Wagner, M. P. Adams, S. Bierbauer, A. K. Bertram, M. Bilde, S. Christiansen, A. M. L. Ekman, E. Gorokhova, K. Höhler, A. A. Kiselev, C. Leck, O. Möhler, B. J. Murray, T. Schiebel, R. Ullrich and M. E. Salter, The ice-nucleating activity of Arctic sea surface microlayer samples and marine algal cultures, *Atmos. Chem. Phys.*, 2020, **20**(18), 11089–11117, DOI: **10.5194/acp-20-11089-2020**.

24 M. Si, E. Evoy, J. Yun, Y. Xi, S. J. Hanna, A. Chivulescu, K. Rawlings, D. Veber, A. Platt, D. Kunkel, *et al.*, Concentrations, composition, and sources of ice-nucleating particles in the Canadian high Arctic during spring 2016, *Atmos. Chem. Phys.*, 2019, **19**(5), 3007–3024, DOI: **10.5194/acp-19-3007-2019**.

25 A. Rocchi, A. von Jackowski, A. Welti, G. Li, Z. A. Kanji, V. Povazhnyy, A. Engel, J. Schmale, A. Nenes, E. Berdalet, R. Simó and M. Dall'Osto, Glucose enhances salinity-driven sea spray aerosol production in eastern Arctic waters, *Environ. Sci. Technol.*, 2024, **58**(20), 8748–8759, DOI: **10.1021/acs.est.4c02826**.

26 N. I. Medina-Pérez, M. Dall'Osto, S. Decesari, M. Paglione, E. Moyano and E. Berdalet, Aerosol toxins emitted by harmful algal blooms susceptible to

complex air–sea interactions, *Environ. Sci. Technol.*, 2020, **55**(1), 468–477, DOI: **10.1021/acs.est.0c05795**.

27 M. van Pinxteren, S. Barthel, K. W. Fomba, K. Müller, W. von Tümpling and H. Herrmann, The influence of environmental drivers on the enrichment of organic carbon in the sea surface microlayer and in submicron aerosol particles – measurements from the Atlantic Ocean, *Elem. Sci. Anth.*, 2017, **5**(06), 35, DOI: **10.1525/elementa.225**.

28 T. Koop and B. Zobrist, Parameterizations for ice nucleation in biological and atmospheric systems, *Phys. Chem. Chem. Phys.*, 2009, **11**, 10839–10850, DOI: **10.1039/B914289D**.

29 R. O. David, M. Cascajo-Castresana, K. P. Brennan, M. Rösch, N. Els, J. Werz, W. Vera, L. S. Boynton, S. Bogler, N. Borduas-Dedekind, C. Marcolli and Z. A. Kanji, Development of the DRoplet Ice Nuclei Counter Zurich (DRINCZ): validation and application to field-collected snow samples, *Atmos. Meas. Tech.*, 2019, **12**, 6865–6888, DOI: **10.5194/amt-12-6865-2019**.

30 G. Vali, Quantitative Evaluation of Experimental Results an the Heterogeneous Freezing Nucleation of Supercooled Liquids, *J. Atmos. Sci.*, 1971, **28**(3), 402–409, DOI: **10.1175/1520-0469(1971)028<0402:QEOERA>2.0.CO;2**.

31 T. Costabloz, F. Burnet, C. Lac, P. Martinet, J. Delanoë, S. Jorquera and M. Fathalli, Vertical profiles of liquid water content in fog layers during the SOFOG3D experiment, *EGUsphere*, 2024, 1–45, DOI: **10.5194/egusphere-2024-1344**.

32 G. Vali, Revisiting the differential freezing nucleus spectra derived from drop-freezing experiments: Methods of calculation, applications, and confidence limits, *Atmos. Meas. Tech.*, 2019, **12**, 1219–1231, DOI: **10.5194/amt-12-1219-2019**.

33 T. C. J. Hill, P. J. DeMott, Y. Tobo, J. Fröhlich-Nowoisky, B. F. Moffett, G. D. Franc and S. M. Kreidenweis, Sources of organic ice nucleating particles in soils, *Atmos. Chem. Phys.*, 2016, **16**(11), 7195–7211, DOI: **10.5194/acp-16-7195-2016**.

34 B. G. Pummer, C. Budke, S. Augustin-Bauditz, D. Niedermeier, L. Felgitsch, C. J. Kampf, R. G. Huber, K. R. Liedl, T. Loerting, T. Moschen, M. Schauperl, M. Tollinger, C. E. Morris, H. Wex, H. Grothe, U. Pöschl, T. Koop and J. Fröhlich-Nowoisky, Ice nucleation by water-soluble macromolecules, *Atmos. Chem. Phys.*, 2015, **15**(8), 4077–4091, DOI: **10.5194/acp-15-4077-2015**.

35 G. Li, J. Wieder, J. T. Pasquier, J. Henneberger and Z. A. Kanji, Predicting atmospheric background number concentration of ice-nucleating particles in the arctic, *Atmos. Chem. Phys.*, 2022, **22**(21), 14441–14454, DOI: **10.5194/acp-22-14441-2022**.

36 R. S. Gilli, C. Karlen, M. Weber, J. Rüegg, K. Barmettler, H. Biester, P. Boivin and R. Kretzschmar, Speciation and mobility of mercury in soils contaminated by legacy emissions from a chemical factory in the Rhône valley in canton of Valais, Switzerland, *Soil Syst.*, 2018, **2**(3), 44, DOI: **10.3390/soilsystems2030044**.

37 N. Hiranuma, S. D. Brooks, R. C. Moffet, A. Glen, A. Laskin, M. K. Gilles, P. Liu, A. M. Macdonald, J. W. Strapp and G. M. McFarquhar, Chemical characterization of individual particles and residuals of cloud droplets and ice crystals collected on board research aircraft in the ISDAC 2008 study, *J. Geophys. Res.:Atmos.*, 2013, **118**(12), 6564–6579, DOI: **10.1002/jgrd.50484**.

38 A. Engel and L. Galgani, The organic sea-surface microlayer in the upwelling region off the coast of Peru and potential implications for air–sea exchange processes, *Biogeosciences*, 2016, **13**(4), 989–1007, DOI: **10.5194/bg-13-989-2016**.
39 A. von Jackowski, J. Grosse, E.-M. Nöthig and A. Engel, Dynamics of organic matter and bacterial activity in the Fram Strait during summer and autumn, *Philos. Trans. R. Soc., A*, 2020, **378**(2181), 20190366, DOI: **10.1098/rsta.2019.0366**.
40 M. Sprenger and H. Wernli, The LAGRANTO Lagrangian analysis tool – version 2.0, *Geosci. Model Dev.*, 2015, **8**(8), 2569–2586, DOI: **10.5194/gmd-8-2569-2015**.
41 H. Wernli and H. C. Davies, A Lagrangian-based analysis of extratropical cyclones. I: The method and some applications, *Q. J. R. Metereol. Soc.*, 1997, **123**(538), 467–489, DOI: **10.1002/qj.49712353811**.
42 H. Hersbach, B. Bell, P. Berrisford, S. Hirahara, A. Horányi, J. Muñoz-Sabater, J. Nicolas, C. Peubey, R. Radu, D. Schepers, A. Simmons, C. Soci, S. Abdalla, X. Abellan, G. Balsamo, P. Bechtold, G. Biavati, J. Bidlot, M. Bonavita, G. De Chiara, P. Dahlgren, D. Dee, M. Diamantakis, R. Dragani, J. Flemming, R. Forbes, M. Fuentes, A. Geer, L. Haimberger, S. Healy, R. J. Hogan, E. Hólm, M. Janisková, S. Keeley, P. Laloyaux, P. Lopez, C. Lupu, G. Radnoti, P. de Rosnay, I. Rozum, F. Vamborg, S. Villaume and J.-N. Thépaut, The ERA5 global reanalysis, *Q. J. R. Metereol. Soc.*, 2020, **146**(730), 1999–2049, DOI: **10.1002/qj.3803**.
43 F. Conen, E. Stopelli and L. Zimmermann, Clues that decaying leaves enrich Arctic air with ice nucleating particles, *Atmos. Environ.*, 2016, **129**, 91–94, DOI: **10.1016/j.atmosenv.2016.01.027**.
44 C. S. McCluskey, T. C. J. Hill, F. Malfatti, C. M. Sultana, C. Lee, M. V. Santander, C. M. Beall, K. A. Moore, G. C. Cornwell, D. B. Collins, K. A. Prather, T. Jayarathne, E. A. Stone, F. Azam, S. M. Kreidenweis and P. J. DeMott, A dynamic link between ice nucleating particles released in nascent sea spray aerosol and oceanic biological activity during two mesocosm experiments, *J. Atmos. Sci.*, 2017, **74**(1), 151–166, DOI: **10.1175/JAS-D-16-0087.1**.
45 H. Wex, L. Huang, W. Zhang, H. Hung, R. Traversi, S. Becagli, R. J. Sheesley, C. E. Moffett, T. E. Barrett, R. Bossi, *et al.*, Annual variability of ice-nucleating particle concentrations at different Arctic locations, *Atmos. Chem. Phys.*, 2019, **19**(7), 5293–5311, DOI: **10.5194/acp-19-5293-2019**.
46 E. K. Bigg and C. Leck, Cloud-active particles over the central Arctic Ocean, *J. Geophys. Res.:Atmos.*, 2001, **106**(D23), 32155–32166, DOI: **10.1029/1999JD901152**.
47 T. M. Seifried, F. Reyzek, P. Bieber and H. Grothe, Scots pines (*Pinus sylvestris*) as sources of biological ice-nucleating macromolecules (INMs), *Atmosphere*, 2023, **14**(2), 266, DOI: **10.3390/atmos14020266**.
48 A. Agresti and B. A. Coull, Approximate is better than "exact" for interval estimation of binomial proportions, *Am. Stat.*, 1998, **52**(2), 119–126.
49 J. M. Creamean, K. J. Suski, D. Rosenfeld, A. Cazorla, P. J. DeMott, R. C. Sullivan, A. B. White, F. M. Ralph, P. Minnis, J. M. Comstock, J. M. Tomlinson and K. A. Prather, Dust and biological aerosols from the Sahara and Asia influence precipitation in the western U.S., *Science*, 2013, **339**(6127), 1572–1578, DOI: **10.1126/science.1227279**.
50 K. R. Barry, T. C. J. Hill, K. A. Moore, T. A. Douglas, S. M. Kreidenweis, P. J. DeMott and J. M. Creamean, Persistence and potential atmospheric

ramifications of ice-nucleating particles released from thawing permafrost, *Environ. Sci. Technol.*, 2023, **57**(9), 3505–3515, DOI: **10.1021/acs.est.2c06530**.

51 J. M. Creamean, T. C. J. Hill, P. J. DeMott, J. Uetake, S. Kreidenweis and T. A. Douglas, Thawing permafrost: an overlooked source of seeds for Arctic cloud formation, *Environ. Res. Lett.*, 2020, **15**(8), 084022, DOI: **10.1088/1748-9326/ab87d3**.

52 G. C. Cornwell, C. M. Sultana, M. Prank, R. E. Cochran, T. C. J. Hill, G. P. Schill, P. J. DeMott, N. Mahowald and K. A. Prather, Ejection of dust from the ocean as a potential source of marine ice nucleating particles, *J. Geophys. Res.:Atmos.*, 2020, **125**(24), e2020JD033073, DOI: **10.1029/2020JD033073**.

53 X. Gong, H. Wex, M. van Pinxteren, N. Triesch, K. W. Fomba, J. Lubitz, C. Stolle, T.-B. Robinson, T. Müller, H. Herrmann and F. Stratmann, Characterization of aerosol particles at Cabo Verde close to sea level and at the cloud level – Part 2: Ice-nucleating particles in air, cloud and seawater, *Atmos. Chem. Phys.*, 2020, **20**(3), 1451–1468, DOI: **10.5194/acp-20-1451-2020**.

54 V. E. Irish, P. Elizondo, J. Chen, C. Chou, J. Charette, M. Lizotte, L. A. Ladino, T. W. Wilson, M. Gosselin, B. J. Murray, *et al.*, Ice-nucleating particles in Canadian Arctic sea-surface microlayer and bulk seawater, *Atmos. Chem. Phys.*, 2017, **17**(17), 10583–10595, DOI: **10.5194/acp-17-10583-2017**.

55 P. J. DeMott, T. C. J. Hill, C. S. McCluskey, K. A. Prather, D. B. Collins, R. C. Sullivan, M. J. Ruppel, R. H. Mason, V. E. Irish, T. Lee, C. Y. Hwang, T. S. Rhee, J. R. Snider, G. R. McMeeking, S. Dhaniyala, E. R. Lewis, J. J. B. Wentzell, J. Abbatt, C. Lee, C. M. Sultana, A. P. Ault, J. L. Axson, M. Diaz Martinez, I. Venero, G. Santos-Figueroa, M. D. Stokes, G. B. Deane, O. L. Mayol-Bracero, V. H. Grassian, T. H. Bertram, A. K. Bertram, B. F. Moffett and G. D. Franc, Sea spray aerosol as a unique source of ice nucleating particles, *Proc. Natl. Acad. Sci. U. S. A.*, 2016, **113**(21), 5797–5803, DOI: **10.1073/pnas.1514034112**.

56 D. B. Collins, A. P. Ault, R. C. Moffet, M. J. Ruppel, L. A. Cuadra-Rodriguez, T. L. Guasco, C. E. Corrigan, B. E. Pedler, F. Azam, L. I. Aluwihare, T. H. Bertram, G. C. Roberts, V. H. Grassian and K. A. Prather, Impact of marine biogeochemistry on the chemical mixing state and cloud forming ability of nascent sea spray aerosol, *J. Geophys. Res.:Atmos.*, 2013, **118**(15), 8553–8565, DOI: **10.1002/jgrd.50598**.

57 A. J. Gabric, B. Qu, P. Matrai and A. C. Hirst, The simulated response of dimethylsulfide production in the Arctic Ocean to global warming, *Tellus B*, 2005, **57**(5), 391–403, DOI: **10.3402/tellusb.v57i5.16564**.

58 C. S. McCluskey, T. C. J. Hill, R. S. Humphries, A. M. Rauker, S. Moreau, P. G. Strutton, S. D. Chambers, A. G. Williams, I. McRobert, J. Ward, M. D. Keywood, J. Harnwell, W. Ponsonby, Z. M. Loh, P. B. Krummel, A. Protat, S. M. Kreidenweis and P. J. DeMott, Observations of ice nucleating particles over Southern Ocean waters, *Geophys. Res. Lett.*, 2018, **45**(21), 11989–11997, DOI: **10.1029/2018GL079981**.

59 L. A. Ladino, J. D. Yakobi-Hancock, W. P. Kilthau, R. H. Mason, M. Si, J. Li, L. A. Miller, C. L. Schiller, J. A. Huffman, J. Y. Aller, D. A. Knopf, A. K. Bertram and J. P. D. Abbatt, Addressing the ice nucleating abilities of marine aerosol: A combination of deposition mode laboratory and field measurements, *Atmos. Environ.*, 2016, **132**, 1–10, DOI: **10.1016/j.atmosenv.2016.02.028**.

60 W. Bruch, J. Piazzola, H. Branger, A. M. J. van Eijk, C. Luneau, D. Bourras and G. Tedeschi, Sea-spray-generation dependence on wind and wave

combinations: A laboratory study, *Bound.-Lay. Meteorol.*, 2021, **180**(3), 477–505, DOI: **10.1007/s10546-021-00636-y**.

61 X. Gong, H. Wex, J. Voigtländer, K. W. Fomba, K. Weinhold, M. van Pinxteren, S. Henning, T. Müller, H. Herrmann and F. Stratmann, Characterization of aerosol particles at Cabo Verde close to sea level and at the cloud level – Part 1: Particle number size distribution, cloud condensation nuclei and their origins, *Atmos. Chem. Phys.*, 2020, **20**(3), 1431–1449, DOI: **10.5194/acp-20-1431-2020**.

62 E. K. Hall, C. Neuhauser and J. B. Cotner, Toward a mechanistic understanding of how natural bacterial communities respond to changes in temperature in aquatic ecosystems, *ISME J.*, 2008, **2**(5), 471–481, DOI: **10.1038/ismej.2008.9**.

63 K. Gao, F. Vogel, R. Foskinis, S. Vratolis, M. I. Gini, K. Granakis, A.-C. Billault-Roux, P. Georgakaki, O. Zografou, P. Fetfatzis, A. Berne, A. Papayannis, K. Eleftheridadis, O. Möhler and A. Nenes, Biological and dust aerosols as sources of ice-nucleating particles in the eastern Mediterranean: source apportionment, atmospheric processing and parameterization, *Atmos. Chem. Phys.*, 2024, **24**(17), 9939–9974, DOI: **10.5194/acp-24-9939-2024**.

64 P. J. DeMott, A. J. Prenni, G. R. McMeeking, R. C. Sullivan, M. D. Petters, Y. Tobo, M. Niemand, O. Möhler, J. R. Snider, Z. Wang and S. M. Kreidenweis, Integrating laboratory and field data to quantify the immersion freezing ice nucleation activity of mineral dust particles, *Atmos. Chem. Phys.*, 2015, **15**, 393–409, DOI: **10.5194/acp-15-393-2015**.

65 M. Niemand, O. Möhler, B. Vogel, H. Vogel, C. Hoose, P. Connolly, H. Klein, H. Bingemer, P. Demott, J. Skrotzki and T. Leisner, A particle-surface-area-based parameterization of immersion freezing on desert dust particles, *J. Atmos. Sci.*, 2012, **69**, 3077–3092, DOI: **10.1175/JAS-D-11-0249.1**.

66 P. J. DeMott, A. J. Prenni, X. Liu, S. M. Kreidenweis, M. D. Petters, C. H. Twohy, M. S. Richardson, T. Eidhammer and D. C. Rogers, Predicting global atmospheric ice nuclei distributions and their impacts on climate, *Proc. Natl. Acad. Sci. U. S. A.*, 2010, **107**, 11217–11222, DOI: **10.1073/pnas.0910818107**.

67 M. Paramonov, S. Drossaart van Dusseldorp, E. Gute, J. P. D. Abbatt, P. Heikkilä, J. Keskinen, X. Chen, K. Luoma, L. Heikkinen, L. Hao, T. Petäjä and Z. A. Kanji, Condensation/immersion mode ice-nucleating particles in a boreal environment, *Atmos. Chem. Phys.*, 2020, **20**(11), 6687–6706, DOI: **10.5194/acp-20-6687-2020**.

68 L. Lacher, M. Steinbacher, N. Bukowiecki, E. Herrmann, A. Zipori and Z. A. Kanji, Impact of air mass conditions and aerosol properties on ice nucleating particle concentrations at the High Altitude Research Station Jungfraujoch, *Atmosphere*, 2018, **9**(9), 363, DOI: **10.3390/atmos9090363**.

69 R. E. Cochran, O. Laskina, T. Jayarathne, A. Laskin, J. Laskin, P. Lin, C. Sultana, C. Lee, K. A. Moore, C. D. Cappa, *et al.*, Analysis of organic anionic surfactants in fine and coarse fractions of freshly emitted sea spray aerosol, *Environ. Sci. Technol.*, 2016, **50**(5), 2477–2486, DOI: **10.1021/acs.est.5b04053**.

70 E. R. Lewis and S. E. Schwartz, *Sea Salt Aerosol Production: Mechanisms, Methods, Measurements, and Models*, American Geophysical Union, 2004, vol. 152.